

The X-ray Transient 2XMMi J003833.3+402133: A Candidate Magnetar at High Galactic Latitude

J. R. Callingham¹, S. A. Farrell^{1,2}, B. M. Gaensler^{1,2}, G. F. Lewis¹, and M. J. Middleton³
¹*Sydney Institute for Astronomy (SfA), School of Physics, The University of Sydney, NSW 2006, Australia*

²*ARC Centre of Excellence for All-sky Astrophysics (CAASTRO)*

³*Department of Physics, University of Durham, South Road, Durham DH1 3LE, UK*

j.callingham@physics.usyd.edu.au

ABSTRACT

We present detailed analysis of the transient X-ray source 2XMMi J003833.3+402133 detected by *XMM-Newton* in January 2008 during a survey of M 31. The X-ray spectrum is well fitted by either a steep power law plus a blackbody model or a double blackbody model. Prior observations with *XMM-Newton*, *Chandra*, *Swift* and *ROSAT* spanning 1991 to 2007, as well as an additional *Swift* observation in 2011, all failed to detect this source. No counterpart was detected in deep optical imaging with the Canada France Hawaii Telescope down to a 3σ lower limit of $g = 26.5$ mag. This source has previously been identified as a black hole X-ray binary in M 31. While this remains a possibility, the transient behaviour, X-ray spectrum, and lack of an optical counterpart are equally consistent with a magnetar interpretation for 2XMMi J003833.3+402133. The derived luminosity and blackbody emitting radius at the distance of M 31 argue against an extragalactic location, implying that if it is indeed a magnetar it is located within the Milky Way but 22° out of the plane. The high Galactic latitude could be explained if 2XMMi J003833.3+402133 were an old magnetar, or if its progenitor was a runaway star that traveled away from the plane prior to going supernova.

Subject headings: Stars: Neutron, X-rays: individual (2XMMi J003833.3+402133), X-rays: stars, Galaxies: individual: M 31

1. Introduction

Magnetars are a rare class of neutron stars which are characterised by a very strong surface magnetic field, typically $10^{14} - 10^{15}$ G (Duncan & Thompson 1992; Woods & Thompson 2006), and relatively slow spin rate ($P \sim 2 - 12$ s) when compared to the majority of observed pulsars. They also differ from normal pulsars in that they are not powered by their spin-down energy losses but by the decay of energy stored in their magnetic field (Duncan & Thompson 1992).

Magnetars are historically divided into two classes: anomalous X-ray pulsars (AXPs) which are characterised by slow pulsations and rapid spin-down, and soft gamma repeaters (SGRs) which exhibit sporadic bursts of hard X-ray/soft

gamma rays. While originally considered to be unrelated, it is now accepted that AXPs and SGRs are the same type of object (Kouveliotou et al. 1998; Gavriil, Kaspi, & Woods 2002; Kaspi et al. 2003). There are currently 16 confirmed magnetars (7 SGRs and 9 AXPs) and a further 7 candidates (4 SGRs and 3 AXPs)¹. Due to this small sample size it is difficult to determine the average lifetime, spatial distribution, duty cycle and luminosity of the population as a whole. However, all the Galactic magnetars lie very close to the Galactic plane, consistent with young ($< 10,000$ yrs) neutron stars with low spatial velocities (< 500 km s^{-1} ; Gaensler et al. 2001). The exceptions are the two magnetars located in the Magellanic Clouds

¹From McGill's Online Catalogue available at <http://www.physics.mcgill.ca/~pulsar/magnetar/main.html>.

(Mazets et al. 1979; McGarry et al. 2005). While there have been reports of the detection of SGRs in M 31 (Ofek et al. 2008; Mazets et al. 2008) and M81 (Frederiks et al. 2007), these sources have been detected only once and their SGR nature has thus yet to be verified.

In this paper we present an in-depth analysis of multi-wavelength data on the X-ray source 2XMMi J003833.3+402133 (hereafter, referred to as XMM J0038+40), which was observed during a survey of the nearby galaxy M 31. Stiele et al. (2011) identified this object (source 57 in their sample) as a probable black hole low-mass X-ray binary (LMXB) located within M 31. Here we argue that the X-ray spectral and timing properties of this source are also consistent with XMM J0038+40 being a new addition to the rare class of Galactic magnetars. If this conclusion is correct, the high Galactic latitude of XMM J0038+40 would make it unique as the other Galactic magnetars are all located within the plane.

2. Data Reduction, Analysis & Results

2.1. X-ray Data

The field of XMM J0038+40 was observed by *XMM-Newton* on 2008 January 2 for 45.5 ks by the three EPIC cameras (pn, MOS1 and MOS2) as part of a survey of the local group galaxy M 31 (Stiele et al. 2011). Source detection performed by the *XMM-Newton* processing pipeline detected a bright uncatalogued source at an off-axis angle of $7.72'$. The source position is RA = $00^{\text{h}}38'33.32''$, dec = $+40^{\circ}21'33.20''$ (J2000) with a 3σ positional uncertainty radius of $1''$ (see Watson et al. (2009) for a detailed description of the source detection procedure). No data were available from the two Reflection Grating Spectrometers (RGS) as XMM J0038+40 fell outside their fields of view.

The Science Analysis System (SAS) version 10.0 software² was used to process the Observation Data Files (ODFs) using the same procedure as outlined by Farrell et al. (2010). Background light curves extracted from the entire field at energies > 10 keV found no evidence for flaring, and so no good time interval filtering was applied. We extracted source spectra using circular regions centred on the source position with radii of $71.5''$ and

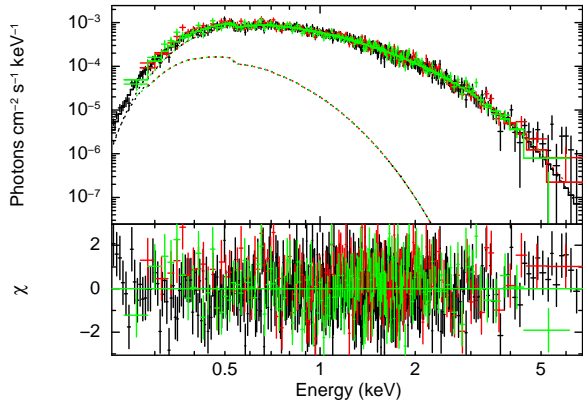


Fig. 1.— *XMM-Newton* unfolded EPIC spectra (black = pn, red = MOS1, green = MOS2) of XMM J0038+40 from the 2008 detection fitted with the Phabs*(DISKBB+CompTT) model. The bottom panel shows the fit residuals.

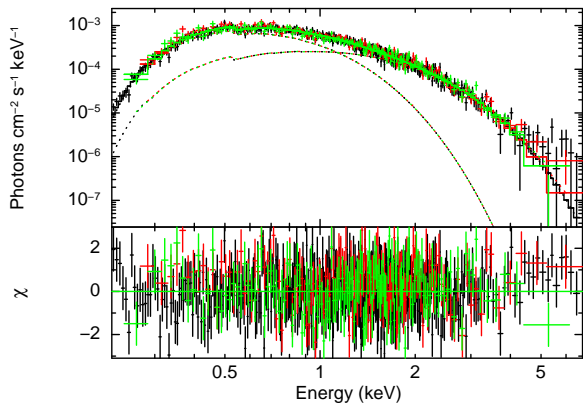


Fig. 2.— *XMM-Newton* unfolded EPIC spectra (black = pn, red = MOS1, green = MOS2) of XMM J0038+40 from the 2008 detection fitted with the Phabs*(BB+BB) model. The bottom panel shows the fit residuals.

²<http://xmm.esa.int/sas/>

41.5'' for the pn and MOS cameras, respectively³. Background spectra were extracted from nearby source-free regions of the field with areas 1.5 times the source extraction region areas. Response and ancillary response files were produced for the spectra and the light curves were corrected using the SAS task *epiclccorr*. The spectra were grouped at 20 counts per bin to provide sufficient statistics for χ^2 fitting and analysed using XSPEC v12.6.0q (Arnaud 1996). Data below 0.2 keV and above 7 keV (where the statistics are very poor) were ignored for the spectral fitting.

2.1.1. X-ray Spectral Analysis

Stiele et al. (2011) fitted spectra extracted from their 2008 *XMM-Newton* observation with three models: absorbed disk blackbody plus power law, absorbed disk blackbody, and absorbed bremsstrahlung models. They found that the disk blackbody plus power law model was the best fitting model obtaining $\chi^2/\text{dof} = 174/145$, although they also claim formally acceptable fits using the two other models (with $\chi^2/\text{dof} = 270/147$ and $209/147$ for the simple disk blackbody and bremsstrahlung models, respectively).

We fitted the spectra we extracted from the 2008 *XMM-Newton* observation with the same models and obtained similar results for the disk blackbody plus power law and the simple disk blackbody models, although we argue that due to the high quality of the data the fit with the simple disk blackbody model is unacceptable with a $\chi^2/\text{dof} = 812/714$. We therefore only report the results of the disk blackbody plus power law fit in Table 1. In contrast, our fit with the absorbed bremsstrahlung model obtained a much better fit ($\chi^2/\text{dof} = 764/714$, see Table 2) with a significantly lower temperature of $kT = 0.98 \pm 0.02$ keV than the $kT = 1.91 \pm 0.07$ keV obtained by Stiele et al. (2011). The cause of the differences between our fitting and that reported by Stiele et al. (2011) is unclear. We also fitted the spectra with a more physical model representing emission from an accreting black hole, i.e. an absorbed disk blackbody plus thermal Comptonisation model (compTT in XSPEC), with the input

soft photon (Wien) temperature fixed to the disk blackbody temperature. Again, we obtained an acceptable fit with $\chi^2/\text{dof} = 746/711$ (see Table 1).

In addition to the model fits reported by Stiele et al. (2011), we attempted to fit the 2008 *XMM-Newton* spectra with power law, blackbody (the BBODYRAD model in XSPEC), and thermal plasma (the MEKAL model in XSPEC; Mewe et al. 1985, 1986; Kaastra 1992; Liedahl et al. 1995) models. In each case photoelectric absorption was accounted for using the phabs component in XSPEC and the Wilms abundances (Wilms, Allen, & McCray 2000). Neither the simple power law model nor blackbody models provided an acceptable fit, with $\chi^2/\text{dof} = 1205/719$ and $1165/719$, respectively, and significant residuals appearing below 2 keV. Adding a low temperature blackbody component to the power law model improved the fit significantly ($\chi^2/\text{dof} = 806/712$), although with a very steep power law photon index (see Table 2). The addition of a second blackbody component to the simple absorbed blackbody model produced a better fit ($\chi^2/\text{dof} = 752/712$) and completely smoothed out the low energy residuals (see Table 2).

Attempts to fit the spectra with an absorbed MEKAL model with the abundance parameter frozen at Solar values did not provide an acceptable fit ($\chi^2/\text{dof} = 11527/719$). Allowing the abundance to vary freely improved the fit significantly ($\chi^2/\text{dof} = 769/718$), however the abundance value fell to zero indicating that no significant line emission is present and therefore the model is consistent with the underlying bremsstrahlung continuum model. In summary, we obtained acceptable fits with the double blackbody, blackbody plus power law, disk blackbody plus power law, disk blackbody plus thermal Comptonisation, and bremsstrahlung models but are able to rule out the simple blackbody, simple power law, and thermal plasma (with non-zero elemental abundances) models. The best fits were obtained with the disk blackbody plus thermal Comptonisation and the double blackbody models, which are shown in Figures 1 and 2.

2.1.2. X-ray Timing Analysis

To search for pulsations in the *XMM-Newton* data, we extracted counts in the energy range 0.2

³The source extraction radii were chosen so as to maximise the signal-to-noise ratio of the data products (V. Braito 2011, private communication).

– 12 keV using the same extraction regions as used for the spectra. This resulted in 8078, 7192 and 23740 counts for the MOS1, MOS2 and pn cameras, respectively. In each case, we corrected the photon arrival times to the Solar system barycenter. To search for high frequency periodic variability we performed a Z_1^2 (Rayleigh) test to search for sinusoidal pulsations (e.g. Leahy et al. 1983). For the MOS1 and MOS2 data, we searched for pulse periods in the range 6.4 to 4500 s, while for pn data we considered periods between 146 ms and 4500 s. We saw no significant power at any period, either in each data set separately or in a period search of all three data sets combined. The corresponding 5σ upper limit on the pulsed fraction is 7% in the period range 146 ms to 6.4 s, and 5.5% in the period range 6.4 to 4500 s.

We also extracted power density spectra (PDS) over the reliable energy bandpass (0.3-6 keV) binned on 10 s. We find that, with linear binning, the variability is consistent with the statistical white noise within 1σ using the most accurate Bayesian least-squares fitting routines (Vaughan 2010). As the shape of the PDS is energy dependent and we could conceivably have a stable, bright component diluting the variability when averaged across the entire bandpass, we also extracted the energy dependent fractional excess variance (see e.g. Edelson et al. 2002; Vaughan et al. 2003). We did this initially for the bands which correspond to the absorbed disk blackbody plus thermal Comptonisation spectral model (0.3 – 0.8 and 0.8 – 6keV; see Figure 1) with binning on 25, 50, 100, 200 and 400 s to test for variability typically seen from black hole X-ray binaries. We could not constrain any variability over any timescales in either energy band above the white noise level, obtaining a 3σ upper limit of 8% on the fractional variability⁴ using the method of van der Klis (1989). This is the theoretical upper limit for what we should be able to detect given the bandpass, count rate, and exposure time. As this relies on our spectral deconvolution being an accurate description of the data we also tested energy bands within these two bands (specifically 0.3 – 0.5, 0.5 – 1, 1 – 2 and 2 – 6 keV) on 400 s binning (to ensure adequate

⁴We note however that this does not take into account the effect of red noise.

statistics in these smaller energy bands) and find no constrained variance above the statistical white noise.

2.1.3. Additional X-ray Observations

M 31 has been observed numerous times previously in X-rays, and thus archival data from *ROSAT*, *XMM-Newton*, *Chandra*, and *Swift* were also analysed. In addition, following the discovery of XMM J0038+40 we obtained Target of Opportunity (ToO) observations of the field with the *Swift* X-ray Telescope (XRT) between 04 – 15 February 2011. For the additional *XMM-Newton* data, we extracted images from all three EPIC cameras after filtering out background flares. Pre-processed images from the archival *Chandra*, *ROSAT*, and *Swift* data were downloaded from NASA’s HEASARC archive⁵. The 2011 *Swift* ToO observation was processed using the online XRT data processing facility⁶ (Evans et al. 2009).

XMM J0038+40 was not detected in any of these data (Figure 3). Upper limits were estimated using the count rates measured within regions centred on the position of XMM J0038+40 in each of the images, subtracted from background count rates measured in nearby source-free regions. The WebPIMMS online flux conversion tool⁷ and the double blackbody spectral model obtained from fitting the EPIC spectra from the 2008 *XMM-Newton* observation were used to convert the 3σ count rate upper limits into flux limits. The flux limits derived in this manner are all well below the flux observed in the 2008 *XMM-Newton* observation indicating that XMM J0038+40 is a transient source with variability by a factor $\gtrsim 450$. Specific details of the observations from which data was analysed including the upper limits of the non-detections are given in the online Appendix (Table A).

2.2. UV, Optical and Near-Infrared Data

XMM J0038+40 fell within the field of view of the Optical Monitor (OM) during all three *XMM-Newton* observations, which observed the field in imaging mode with the *uvw1* and *uvm2* UV fil-

⁵<http://heasarc.gsfc.nasa.gov/cgi-bin/W3Browse/w3browse.pl>

⁶http://www.swift.ac.uk/user_objects/

⁷<http://heasarc.gsfc.nasa.gov/Tools/w3pimms.html>

Table 1: Best fit spectral parameters to the 2008 *XMM-Newton* observation of XMM J0038+40 fitted with disk blackbody plus power law, and disk blackbody plus thermal Comptonisation models.

Parameter	DISKBB+Pow ^a	DISKBB+CompTT ^a	Units
N_H	$0.13^{+0.1}_{-0.02}$	$0.11^{+0.05}_{-0.03}$	10^{22} cm^{-2}
kT_1 ^b	0.46 ± 0.01	$0.17^{+0.2}_{-0.02}$	keV
Norm ₁ ^c	$2.2^{+0.2}_{-0.3}$	16^{+39}_{-16}	...
Γ/T_0 ^d	$2.4^{+0.9}_{-0.5}$	$0.17^{+0.2}_{-0.02}$... /keV
kT_2 ^e	...	0.50 ± 0.03	keV
τ ^f	...	14^{+2}_{-1}	...
Norm ₂ ^g	$8^{+30}_{-5} \times 10^{-5}$	$4^{+1}_{-3} \times 10^{-3}$...
Flux _{abs} ^h	1.53 ± 0.02	1.48 ± 0.02	$10^{-12} \text{ erg cm}^{-2} \text{ s}^{-1}$
Flux _{unabs} ^h	$2.7^{+3.0}_{-0.4}$	$2.08^{+0.5}_{-0.3}$	$10^{-12} \text{ erg cm}^{-2} \text{ s}^{-1}$
Flux ₁ /Flux ₂ ⁱ	2.37	0.10	...
χ^2/dof	778/712	746/711	...

^aAll models include an absorption component. Errors are quoted at the 90% confidence level.

^bTemperature of the first model component.

^cNormalisation of the first model component.

^dThis row contains the photon index for the power law component in the DISKBB+POW model and the soft photon temperature (T_0) for the thermal Comptonisation component in the DISKBB+CompTT model.

^ePlasma temperature of the thermal Comptonisation model component.

^fPlasma optical depth.

^gNormalisation of the second model component.

^hAbsorbed and unabsorbed fluxes are calculated over the energy range 0.2 – 10 keV.

ⁱRatio of unabsorbed 0.2 – 10 keV fluxes of model component 1 over model component 2.

Table 2: Best fit spectral parameters to the 2008 *XMM-Newton* observation of XMM J0038+40 fitted with the bremsstrahlung, double blackbody and blackbody plus power law models.

Parameter	Bremsstrahlung	BB+BB ^a	BB+Pow ^a	Units
N_H	0.194 ± 0.006	0.08 ± 0.01	$0.35^{+0.02}_{-0.01}$	10^{22} cm^{-2}
kT_1 ^b	0.98 ± 0.02	0.207 ± 0.005	0.37 ± 0.01	keV
Norm ₁ ^c	$1.72 \pm 0.06 \times 10^{-3}$	48^{+18}_{-11}	$4.1^{+1.0}_{-0.7}$...
kT_2/Γ ^d	...	$0.44^{+0.01}_{-0.02}$	$3.7^{+0.2}_{-0.1}$	keV/ ...
Norm ₂ ^e	...	$2.5^{+0.7}_{-0.6}$	$7.8^{+0.7}_{-0.8} \times 10^{-4}$...
Flux _{abs} ^f	1.51 ± 0.02	1.50 ± 0.02	1.50 ± 0.02	$10^{-12} \text{ erg cm}^{-2} \text{ s}^{-1}$
Flux _{unabs} ^f	$3.18^{+0.07}_{-0.06}$	$1.90^{+0.10}_{-0.08}$	12^{+3}_{-2}	$10^{-12} \text{ erg cm}^{-2} \text{ s}^{-1}$
Flux ₁ /Flux ₂ ^g	...	0.94	0.07	...
χ^2/dof	764/714	752/712	806/712	...

^aAll models include an absorption component. Errors are quoted at the 90% confidence level.

^bTemperature of the first model component.

^cNormalisation of the first model component.

^dThis row contains the temperature for the second BB component in the BB+BB model and the photon index of the power law component in the BB+Pow model.

^eNormalisation of the second model component.

^fAbsorbed and unabsorbed fluxes are calculated over the energy range 0.2 – 10 keV.

^gRatio of unabsorbed 0.2 – 10 keV fluxes of model component 1 over model component 2.

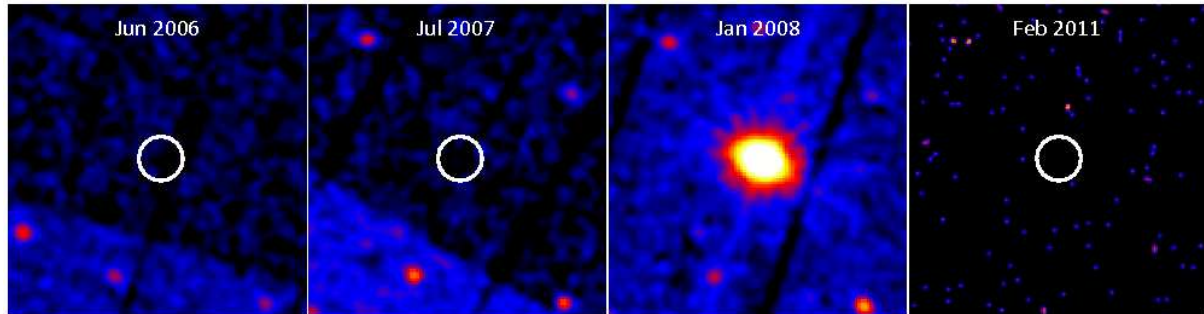


Fig. 3.— X-ray images of the field of XMM J0038+40 taken with *XMM-Newton* (panels 1 to 3 from the left) and *Swift*. The white circle indicates the position of XMM J0038+40 with a radius of $30''$. The *XMM-Newton* images span the energy range of 0.2 – 12 keV, while the *Swift* image spans 0.3 – 10 keV. A Gaussian smoothing function with a kernel radius of 3 pixels was applied to all images.

ters. As the 2008 OM images are the only available UV data that were taken at the time when XMM J0038+40 was X-ray bright, we focused on these data for our analysis (though we note that no source was detected within the X-ray error circle in any of the other OM or *Swift* UVOT data). The total exposure times during this observation were 1461 s and 6317 s for the *uvw1* and *uvm2* filters, respectively. No source was detected within the 3σ X-ray error circle of XMM J0038+40 in any of the images. We determined 3σ count rate upper limits at the position of XMM J0038+40 using the *XMM-Newton* pipeline processed images and the same method as that used for the X-ray non-detections, and converted the count rates into Vega magnitudes using the filter zero points for the OM⁸.

Deep *g*- and *i*-band images of the field of XMM J0038+40 were taken with the Canada France Hawaii Telescope (CFHT) on 2008 October 3 as part of the Pan-Andromeda Archaeological Survey (PAndAS; McConnachie et al. 2009). The CFHT observations and data reduction procedures are described by Ibata et al. (2007). No counterpart was detected in either band image within the X-ray error circle of XMM J0038+40 (see Figure 4), so we determined magnitude lower limits in the same manner as described above. There is however a faint point source just outside and to the South-East of the error circle at RA = $00^{\text{h}}38^{\text{m}}33.3^{\text{s}}$, dec = $+40^{\circ}21'31.9''$ with $g = 24.3 \pm$

0.1 mag and $i = 22.11 \pm 0.04$ mag which could possibly be the counterpart. No source was present within or even nearby the X-ray error circle in the 2MASS J, H, and K_s images. In order to estimate conservative magnitude lower limits in the 2MASS near-infrared (NIR) data, we identified the faintest source in each band within $30'$ of XMM J0038+40 and adopted these magnitudes as the lower limits. All the lower limits derived from the UV, optical and NIR data are given in Table 3.

2.3. Radio Data

The region surrounding XMM J0038+40 has been imaged at various radio frequencies as part of surveys of M 31. Using these data, we find no radio source at the position of XMM J0038+40 at frequencies of 0.3, 0.6 or 1.4 GHz, with 5σ upper limits on the flux of a radio counterpart of 5, 4 and 1.5 mJy, respectively (Bystedt et al. 1984; Walterbos et al. 1985; Gelfand et al. 2004). Less sensitive observations at 0.3 and 1.4 GHz at other epochs also show no radio source at this position (Rengelink et al. 1997; Condon et al. 1998).

3. Discussion & Conclusions

The X-ray spectrum, transient behaviour, and lack of an optical and infrared counterpart place strong constraints on the nature of XMM J0038+40. Non-transient objects such as isolated cooling neutron stars and rotation powered pulsars with moderate magnetic field strengths can immediately be ruled out, leaving behind objects that are known to exhibit large scale variability.

⁸http://xmm.esa.int/external/xmm_user_support/documentation/uint9_1295/uint9_1295.html

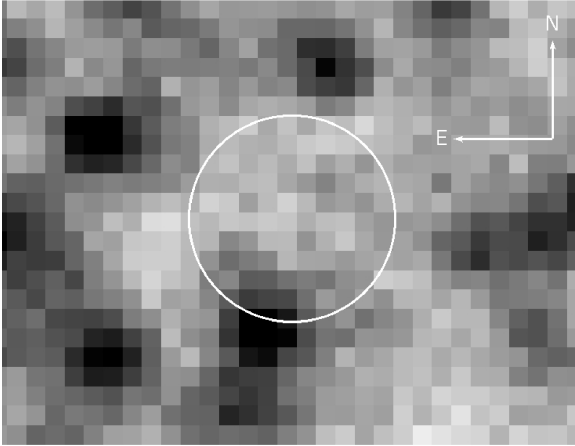


Fig. 4.— CFHT g -band image with the X-ray position of XMM J0038+40 indicated by the white circle, with a radius equal to the 3σ positional error of $1''$.

Table 3: UV, Optical and NIR Lower Limits

Telescope/ Survey	Filter	Date	Lower Limit (mag)
OM	<i>uvw1</i>	2008-01-02	20.1
OM	<i>uvm2</i>	2008-01-02	19.3
CFHT	g	2008-10-03	26.5
CFHT	i	2008-10-03	25.5
2MASS	J	2000-10-25	17.7
2MASS	H	2000-10-25	16.6
2MASS	K_s	1998-12-04	16.3

Although the CFHT optical imaging was not taken at the same time as XMM J0038+40 was detected in X-rays, we would still expect to detect an optical counterpart consistent with the X-ray source position if XMM J0038+40 were a star, a cataclysmic variable (CV) or an Active Galactic Nucleus (AGN). The X-ray detection and deep g -band and i -band limits indicate X-ray to optical flux ratios of $F_X/F_g \geq 8200$ and $F_X/F_i \geq 5800$ for XMM J0038+40. Even if the source just outside the *XMM-Newton* error circle were the counterpart the flux ratios would be $F_X/F_g \sim 1300$ and $F_X/F_i \sim 340$. These are far in excess of the ratios observed for AGN and stars, which typically have X-ray to optical flux ratios of $F_X/F_O < 10$ and < 0.01 , respectively (e.g. Mainieri et al. 2002). It is also inconsistent with CVs which typically have $F_X/F_O \leq 0.1$ (Kuulkers et al. 2006).

High levels of dust extinction could explain the lack of an optical counterpart⁹, however the position of XMM J0038+40 $\sim 22^\circ$ out of the Galactic plane puts it in a region of low dust extinction with $E(B-V) = 0.062$ mag (Schlegel et al. 1998). The weighted average Galactic neutral hydrogen absorption in the direction of XMM J0038+40 as measured by the Leiden/Argentine/Bonn (LAB) survey of Galactic HI is $7.6 \times 10^{20} \text{ cm}^{-2}$ (Kalberla et al. 2005), consistent with the N_H values determined through the X-ray spectral fitting (i.e. $8 - 35 \times 10^{20} \text{ cm}^{-2}$, Tables 1 & 2) with some additional intrinsic absorption¹⁰. If XMM J0038+40 is located within or behind M 31 there may be an additional contribution from the galaxy disk. However, the low N_H values from the X-ray spectral fitting indicate that M 31 is unlikely to be a major contributor to the extinction. We thus conclude that the high flux ratio is not due to dust reddening.

The lack of a point-like radio counterpart above 1.5 mJy is not very constraining. For example, using the black hole fundamental plane relationship between X-ray luminosity, radio luminosity, and black hole mass, we would not expect to be

⁹But not the lack of a NIR counterpart in the 2MASS images.

¹⁰We note that the N_H of the blackbody plus power law model was higher than the other models and a factor of ~ 5 above the Galactic value (still consistent with a moderate level of intrinsic absorption). The N_H and power law photon index are degenerate in the fit, so the parameters of this model are likely to be untrustworthy.

able to detect radio emission from an AGN unless it was closer than 1.5 Mpc (assuming a black hole mass of $10^6 M_{\odot}$; e.g. K rding et al. 2006). At such a distance the galaxy itself should be easily resolved in the optical/NIR images. Likewise, radio emission from the jet of a $20 M_{\odot}$ black hole X-ray binary would not be detectable unless the system was closer than 20 pc, a distance at which emission from the disk or donor star would surely be detectable in our deep optical images.

The EPIC X-ray spectra are consistent with blackbody plus steep power law, double blackbody, disk blackbody plus power law, disk blackbody plus thermal Comptonisation, or thermal bremsstrahlung models (all with the addition of a photoelectric absorption component of low column density, consistent with the Galactic latitude of the source). The temperature of the bremsstrahlung model was 0.98 keV, much lower than the lowest temperature measured for a CV (kT = 1.9 keV from thermal plasma fits to *XMM-Newton* spectra of the quiescent dwarf nova GW Lib; Hilton et al. 2007). In addition, line emission becomes more significant relative to the underlying continuum spectrum for CVs with low temperature spectra. Hence, if XMM J0038+40 was a CV it would be expected that the spectrum would be consistent with a thermal plasma model with non-zero elemental abundances. The spectrum of XMM J0038+40 is not consistent with such a model, adding further weight to the argument against it being a CV.

Spectra of accreting black hole and neutron star X-ray binaries are typically modelled by a power law (representing inverse Compton emission), sometimes with the addition of a soft thermal component attributed either to emission from the surface (in the case of a neutron star) or the accretion disk (e.g. Remillard & McClintock 2006; Orlandini 2006). Observationally it can be difficult to discriminate between black hole and neutron stars in X-ray binaries unless the compact object undergoes behaviour such as thermonuclear bursts or spin period pulsations that are definitively identified with neutron stars. However, a clear separation between neutron star and black hole X-ray binaries has been found empirically in the *XMM-Newton* hardness ratios, particularly evident in the medium and hard X-ray bands (Farrell et al. 2012, in preparation). This separa-

tion was previously noted by Done et al. (2007) in *RXTE* data and attributed to the presence of a surface in neutron stars and an event horizon in black holes. When compared with a sample of neutron star and black hole X-ray binaries drawn from the 2XMM catalogue the hardness ratios of XMM J0038+40 place it in the parameter space populated by black hole X-ray binaries. The only neutron star systems that have spectra as soft are the rare class of quiescent neutron star X-ray binaries. The spectra of these objects are dominated by thermal emission from the surface or atmosphere of the neutron star (with a faint Compton tail; Campana & Stella 2004, and references therein), which is inconsistent with the spectral fitting of XMM J0038+40 (see Table 2).

We now consider the possibility that XMM J0038+40 is a black hole X-ray binary. The temperature derived for the disk blackbody components when fitting the EPIC spectra with the disk blackbody plus power law model (see Table 1) is significantly less than that generally seen in black hole binary spectra when the disk is inferred to be at the inner stable circular orbit (ISCO; see the reviews of e.g. McClintock & Remillard 2006; Done et al. 2007). Such a low temperature is most consistent with black hole binaries that are not in the disk dominated spectral state but are instead transitioning to the low/hard state where the disk does not extend to the ISCO. If the disk is truncated at the lowest mass accretion rates (see Maccarone 2003) then the temperature of this component should be lower and the spectrum should be appended by a strong, hard tail of emission (McClintock & Remillard 2006). This tail is accompanied by large amounts of variability on all timescales (although this variability itself may originate in the disk: see Uttley et al. 2011), inconsistent with the absence of variability in the EPIC light curves of XMM J0038+40.

While such low disk temperatures are most often seen in conjunction with variability, there are cases where it is not. One example is the black hole X-ray binary XTE J1752-223, which has been observed to have a disk temperature as low as 0.5 keV with < 20% RMS variability before beginning the transition to the low/hard state (Curran et al. 2011). The lack of variability and the low disk temperature does not therefore rule out XMM J0038+40 as a black hole X-ray binary. The lumi-

nosity of XTE J1752-223 while it displayed a disk temperature of ~ 0.5 keV was $\sim 2 \times 10^{37}$ erg s $^{-1}$ in the 0.2 – 10 keV band (assuming the distance of 3.5 kpc derived by Shaposhnikov et al. 2010). In comparison, XMM J0038+40 has a luminosity of $\sim 2 \times 10^{38}$ erg s $^{-1}$ if it is located in M 31 ($D \sim 0.8$ Mpc), indicating that (if it is a black hole X-ray binary) it makes the transition from the high/soft to low/hard spectral states at an Eddington fraction a factor of 10 higher than XTE J1752-223. Alternatively, if XMM J0038+40 is located within our own Galaxy, its luminosity would be $< 4 \times 10^{34}$ erg s $^{-1}$ (assuming a distance < 15 kpc), far too low for a black hole X-ray binary in the high/soft state and therefore favouring a location within M 31. However, if XMM J0038+40 is a black hole binary in M 31 it is located in an unusual environment. All the known M 31 X-ray binaries and candidates are either located in globular clusters or within the dusty star forming rings (Stiele et al. 2011). In contrast, XMM J0038+40 is not coincident with a globular cluster and is found well outside the star forming ring (see Figure 5), indicating that it must have been ejected from its birth location. The angular distance from XMM J0038+40 to the nearest star forming ring is $\sim 8.5'$, implying a minimum distance of ~ 2 kpc at the distance of M 31. Adopting a kick velocity of 500 km s $^{-1}$ from the supernova explosion that formed the black hole, we derive a travel time of > 4 Myr, well within the project lifetime of a low mass donor star.

We now consider the possibility that XMM J0038+40 could be a magnetar. The X-ray spectra of magnetars have been historically fitted with a two component model comprised of a steep power law plus a blackbody (e.g. Marsden & White 2001)¹¹. However, Halpern & Gotthelf (2005) argue that this model is not physically justified and favour the fitting of a double blackbody model. They emphasize this is more physically feasible as the pulse modulation of the magnetar can be

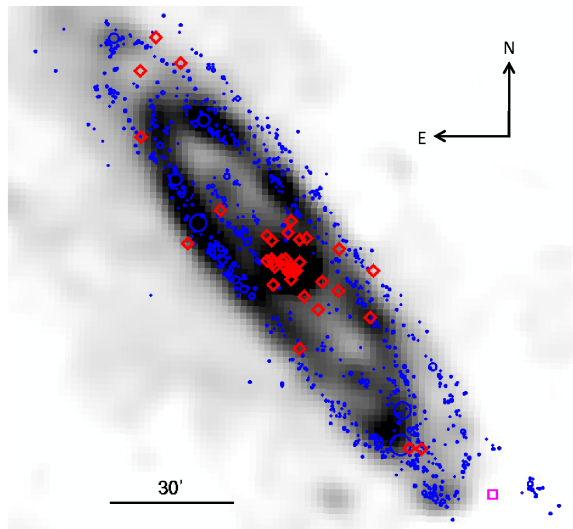


Fig. 5.— IRAS 60 μ m image of M 31 with the distribution of star forming regions (blue circles; Kang et al. 2009) plus X-ray binaries and candidates from the XMM LP-total catalogue (red diamonds; Stiele et al. 2011) over-plotted. All the X-ray binaries are located within the dusty star forming rings of M 31 except for XMM J0038+40 (purple square), which is distinctly removed from any nearby regions of star formation.

¹¹We caution that this is not a physical representation, and that the power law component is invoked simply to fit the high-energy residuals that the blackbody component does not account for. While the blackbody temperature might have some physical meaning for sources with reasonable absorption, for sources with low absorption such as XMM J0038+40 the power law blows up at low-energy and the temperature of the blackbody fit is probably not meaningful.

understood in terms of anisotropic heat conduction and radiative transfer in the strong magnetic field. The EPIC spectra of XMM J0038+40 are consistent with both the blackbody plus steep power law and the double blackbody models, with the spectral parameters falling well within the range spanned by SGRs and AXPs (e.g. Marsden & White 2001). The absence of slow pulsations in the light curve of XMM J0038+40 (one of the defining characteristics of magnetars) does not weigh against the magnetar hypothesis, as pulsed fractions below the upper limit of 7% derived for XMM J0038+40 have been observed from other magnetars (e.g. the AXP 4U 0142+614 has been observed with a pulsed fraction as low as $\sim 5\%$; Rea et al. 2007).

Magnetars typically have very faint or no counterparts in NIR and optical wavelengths (e.g. Hulleman et al. 2000; Gelfand & Gaensler 2007), consistent with the deep limits we have obtained for XMM J0038+40. In particular, using the unabsorbed X-ray flux and the 2MASS K_s band magnitude limit, the X-ray to NIR flux ratio for XMM J0038+40 is $F_X/F_{K_s} > 37$, which is consistent with the flux ratios of the known magnetars (see e.g. Figure 5 of Gelfand & Gaensler 2007). The X-ray variability by a factor of $\gtrsim 450$ observed from XMM J0038+40 is of the same order as seen from other magnetars (e.g. XTE J1810–197, CXOU J164710.2–455216, and AX J1845.0–0258; see e.g. Tam et al. 2006; Albano et al. 2010, and references therein) but slightly higher than the most extreme example (AX J1845.0–0258 with a variability factor of 260 – 430; Tam et al. 2006). Thus, the X-ray spectrum, transient behaviour, and high F_X/F_O ratio are all consistent with the known sample of magnetars.

Apart from the two magnetars located in the Magellanic Clouds, all the other members of this class have been found very close to the plane of our own Galaxy. In contrast, XMM J0038+40 is coincident with the outer edges of the nearby galaxy M 31. The 0.2 – 10 keV X-ray luminosity of XMM J0038+40 at the distance of M 31 is $\sim 2 \times 10^{38}$ erg s $^{-1}$, about 3 orders of magnitude higher than typically seen from magnetars following an outburst (Rea & Esposito 2011). In addition, if XMM J0038+40 is located in M 31, the radius of the blackbody emitting radii derived from the normalization of the BBODYRAD com-

ponents are 554 km and 126 km for the double blackbody model and 162 km for the blackbody plus power law model. These radii are far greater than the maximum radius of a neutron star. When taken in conjunction with the unusually high luminosity, we conclude that XMM J0038+40 is unlikely to be a magnetar located within M 31, and (if it is a magnetar) is most likely to be Galactic.

If XMM J0038+40 is $< 10,000$ yr old with a spatial velocity < 500 km s $^{-1}$, assuming it was born in a supernova explosion from a massive star in the Galactic plane (e.g. Gaensler et al. 2001), then it could only have travelled ~ 5 pc directly out of the plane. The Galactic latitude of $b \sim 22^\circ$ therefore implies a line-of-sight distance of ~ 13 pc, making XMM J0038+40 an improbably nearby magnetar. Furthermore, the derived luminosity at such a distance is only $\sim 5 \times 10^{27}$ erg s $^{-1}$, significantly lower than typically observed from magnetars. If the luminosity of XMM J0038+40 is between $10^{32} - 10^{35}$ erg s $^{-1}$ like the other magnetars, this implies a distance of between $\sim 0.7 - 21$ kpc from Earth and therefore a distance of $\sim 0.3 - 8$ kpc from the Galactic plane. This then implies either an implausibly high spatial velocity $> 10,000$ km s $^{-1}$ (for an age $< 10,000$ yr) or an age $> 3 \times 10^6$ yr (for a spatial velocity < 500 km s $^{-1}$).

Such an age is inconsistent with that derived for magnetars. However, SGR-like behaviour has been observed from a source (SGR 0418+5729) located at a moderate Galactic latitude ($b = +5.1^\circ$). Pulsations with a period of ~ 9.1 s have been detected from SGR 0418+5729 but with a very small period derivative of $\dot{P} < 6 \times 10^{-15}$ s s $^{-1}$, implying a surface dipolar magnetic field strength of $< 7.5 \times 10^{12}$ G and a characteristic age of $> 24 \times 10^6$ yr (Rea et al. 2010). Thus, if the progenitor of XMM J0038+40 was a massive star that went supernova within the Galactic plane, it is possible that it is an old magnetar where the magnetic field strength has decayed to $\sim 10^{12}$ G.

Alternatively, the high Galactic latitude of XMM J0038+40 could be explained by the progenitor being a massive runaway star that originated in a binary system that became unbound, and then travelled outside the plane of the Galaxy prior to going supernova. Runaway O and B-type stars have been observed in our Galaxy with space velocities up to ~ 100 km s $^{-1}$ (Hoogerwerf et al. 2001). Assuming a similar space velocity, the

progenitor of XMM J0038+40 would have taken $\sim 3 \times 10^6 - 8 \times 10^7$ yr to travel $\sim 0.3 - 8$ kpc out of the Galactic plane (assuming a velocity vector perpendicular to the plane). These timescales are perfectly consistent with the nuclear burning lifetimes of massive stars with masses between $\sim 8 - 30 M_{\odot}$ with lifetimes between $\sim 7 - 40 \times 10^6$ yr (Maeder & Meynet 1989).

In order to discriminate between a black hole X-ray binary and a magnetar, we need to either detect spectral state transitions (that are the signature of black hole binaries) or pulsations (that are a signature of magnetars). If the pulsations are detected, the measurement of the spin derivative would then allow us to derive both the surface dipole magnetic field strength and the characteristic age of the neutron star, discriminating between the two possibilities we describe above for the nature of the magnetar. Further deep X-ray observations triggered based on regular monitoring of XMM J0038+40 are thus required.

We thank the anonymous referee for their comments which improved the paper, and Jeff McClintock for useful discussions. JRC acknowledges the support of a vacation scholarship from the School of Physics at The University of Sydney. SAF is the recipient of an Australian Research Council Post Doctoral Fellowship, funded by grant DP110102889. Parts of this research were conducted by the Australian Research Council Centre of Excellence for All-sky Astrophysics (CAASTRO), through project number CE110001020. GFL thanks the Australian Research Council for support through his Future Fellowship (FT100100268) and Discovery Project (DP110100678). MJM thanks STFC for their support in the form of a postdoctoral position funded by a standard grant. We thank Neil Gehrels and the *Swift* team for the follow-up Target of Opportunity observation. Based on observations from XMM-Newton, an ESA science mission with instruments and contributions directly funded by ESA Member States and NASA. This work made use of the 2XMM Serendipitous Source Catalogue, constructed by the XMM-Newton Survey Science Centre on behalf of ESA. We also thank the Pan-Andromeda Archaeological Survey (PANdAS) collaboration for kindly providing the CFHT data. This publication makes use of data products

from the Two Micron All Sky Survey, which is a joint project of the University of Massachusetts and the Infrared Processing and Analysis Center/California Institute of Technology, funded by the National Aeronautics and Space Administration and the National Science Foundation. The Centre for All-sky Astrophysics is an Australian Research Council Centre of Excellence, funded by grant CE11E0090.

Facilities: XMM-Newton (EPIC).

REFERENCES

- Albano, A., Turolla, R., Israel, G. L., Zane, S., Nobili, L., & Stella, L. 2010, *ApJ*, 722, 788
- Arnaud, K. A. 1996, *Astronomical Data Analysis Software and Systems V*, 101, 17
- Bradley, C. K., Hynes, R. I., Kong, A. K. H., Haswell, C. A., Casares, J., & Gallo, E. 2007, *ApJ*, 667, 427
- Bystedt, J. E. V., Brinks, E., de Bruyn, A. G., Israel, F. P., Schwope, P. B. W., Shane, W. W., & Walterbos, R. A. M. 1984, *A&AS*, 56, 245
- Campana, S., & Stella, L. 2004, *NuPhS*, 132, 427
- Condon, J. J., Cotton, W. D., Greisen, E. W., Yin, Q. F., Perley, R. A., Taylor, G. B., & Broderick, J. J. 1998, *AJ*, 115, 1693
- Curran, P. A., Maccarone, T. J., Casella, P., et al. 2011, *MNRAS*, 410, 541
- Duncan, R. C. & Thompson, C. 1992, *ApJ*, 392, L9
- Done, C., Gierliński, M., & Kubota, A. 2007, *A&A Rev.*, 15, 1
- Edelson, R., Turner, T. J., Pounds, K., Vaughan, S., Markowitz, A., Marshall, H., Dobbie, P., & Warwick, R. 2002, *ApJ*, 568, 610
- Evans, P. A., et al. 2009, *MNRAS*, 397, 1177
- Farrell, S. A., Gosling, A. J., Webb, N. A., Barret, D., Rosen, S. R., Sakano, M., & Pancrazi, B. 2010, *A&A*, 523, A50
- Frederiks, D. D., Palshin, V. D., Aptekar, R. L., Golenetskii, S. V., Cline, T. L., & Mazets, E. P. 2007, *AstL*, 33, 19

- Gaensler, B. M., Slane, P. O., Gotthelf, E. V., & Vasisht, G. 2001, *ApJ*, 559, 963
- Gavriil, F. P., Kaspi, V. M., & Woods, P. M. 2002, *Nature*, 419, 142
- Gelfand, J. D., Lazio, T. J. W., & Gaensler, B. M. 2004, *ApJS*, 155, 89
- Gelfand, J. D., & Gaensler, B. M. 2007, *ApJ*, 667, 1111
- Halpern, J. P. & Gotthelf, E. V. 2005, *ApJ*, 618, 874
- Hilton, E. J., Szkody, P., Mukadam, A., Mukai, K., Hellier, C., van Zyl, L., & Homer, L. 2007, *AJ*, 134, 1503
- Hoogerwerf, R., de Bruijne, J. H. J., & de Zeeuw, P. T. 2001, *A&A*, 365, 49
- Hulleman, F., van Kerkwijk, M. H., & Kulkarni, S. R. 2000, *Nature*, 408, 689
- Hynes, R. I., et al. 2004, *ApJ*, 611, L125
- Ibata, R., Martin, N. F., Irwin, M., Chapman, S., Ferguson, A. M. N., Lewis, G. F., & McConnachie, A. W. 2007, *ApJ*, 671, 1591
-]Kaastra, J.S. 1992, An X-Ray Spectral Code for Optically Thin Plasmas (Internal SRON-Leiden Report, updated version 2.0)
- Kalberla, P. M. W., Burton, W. B., Hartmann, D., Arnal, E. M., Bajaja, E., Morras, R., Pöppel, W. G. L. 2005, *A&A*, 440, 775
- Kang, Y., Bianchi, L., & Rey, S.-C. 2009, *ApJ*, 703, 614
- Kaspi, V. M., Gavriil, F. P., Woods, P. M., Jensen, J. B., Roberts, M. S. E., & Chakrabarty, D. 2003, *ApJ*, 588, L93
- Körding, E., Falcke, H., & Corbel, S. 2006, *A&A*, 456, 439
- Kouveliotou, C., et al. 1998, *Nature*, 393, 235
- Kuulkers, E., Norton, A., Schwobe, A., & Warner, B. 2006, *Compact stellar X-ray sources*, 421
- Leahy, D. A., Elsner, R. F., & Weisskopf, M. C. 1983, *ApJ*, 272, 256
- Liedahl, D. A., Osterheld, A. L., & Goldstein, W. H. 1995, *ApJ*, 438, L115
- Maccarone, T. J. 2003, *A&A*, 409, 697
- Maeder, A., & Meynet, G. 1989, *A&A*, 210, 155
- Mainieri, V., Bergeron, J., Hasinger, G., Lehmann, I., Rosati, P., Schmidt, M., Szokoly, G., & Della Ceca, R. 2002, *A&A*, 393, 425
- Marsden, D., & White, N. E. 2001, *ApJ*, 551, L155
- Mazets, E. P., Golentskii, S. V., Ilinskii, V. N., Aptekar, R. L., & Guryan, Iu. A. 1979, *Nature*, 282, 587
- Mazets, E. P., et al. 2008, *ApJ*, 680, 545
- McClintock, J. E., & Remillard, R. A. 2006, *Compact stellar X-ray sources*, 157
- McConnachie, A. W., et al. 2009, *Nature*, 461, 66
- McGarry, M. B., Gaensler, B. M., Ransom, S. M., Kaspi, V. M., & Veljkovic, S. 2005, *ApJ*, 627, L137
- Mewe, R., Gronenschild, E. H. B. M., & van den Oord, G. H. J. 1985, *A&AS*, 62, 197
- Mewe, R., Lemen, J. R., & van den Oord, G. H. J. 1986, *A&AS*, 65, 511
- Narayan, R., Kato, S., & Honma, F. 1997, *ApJ*, 476, 49
- Ofek, E. O., et al. 2008, *ApJ*, 681, 1464
- Orlandini, M. 2006, *AdSpR*, 38, 2742
- Rea, N., et al. 2007, *MNRAS*, 381, 293
- Rea, N., et al. 2010, *Science*, 330, 944
- Rea, N., & Esposito, P. 2011, *High-Energy Emission from Pulsars and their Systems*, 247
- Remillard, R. A., & McClintock, J. E. 2006, *ARA&A*, 44, 49
- Rengelink, R. B., Tang, Y., de Bruyn, A. G., Miley, G. K., Bremer, M. N., Roettgering, H. J. A., & Bremer, M. A. R. 1997, *A&AS*, 124, 259 & Zavlin, V. E. 2000, *ApJ*, 529, 985
- Schlegel, D. J., Finkbeiner, D. P., & Davis, M. 1998, *ApJ*, 500, 525

- Shaposhnikov, N., Markwardt, C., Swank, J., & Krimm, H. 2010, *ApJ*, 723, 1817
- Stiele, H., Pietsch, W., Haberl, F., et al. 2011, *A&A*, 534, A55
- Tam, C. R., Kaspi, V. M., Gaensler, B. M., & Gotthelf, E. V. 2006, *ApJ*, 652, 548
- Uttley, P., Wilkinson, T., Cassatella, P., Wilms, J., Pottschmidt, K., Hanke, M., Böck, M. 2011, *MNRAS*, 414, L60
- van der Klis, M. 1989, in *Timing neutron stars*, ed. H. Ögelman & E. P. J. van den Heuvel (New York, USA: Kluwer Academic/Plenum Publishers), 27
- Vaughan, S., Edelson, R., Warwick, R. S., & Uttley, P. 2003, *MNRAS*, 345, 1271
- Vaughan, S. 2010, *MNRAS*, 402, 307
- Walterbos, R. A. M., Brinks, E., & Shane, W. W. 1985, *A&AS*, 61, 451
- Watson, M. G., et al. 2009, *A&A*, 493, 339
- Wilms, J., Allen, A. & McCray, R. 2000, *ApJ*, 542, 914
- Woods, P. M., & Thompson, C. 2006, in *Compact stellar X-ray sources*, ed. W. Lewin & M. van der Klis (Cambridge, UK: Cambridge University Press), 547

A. Details of X-ray Observations

Table A lists the details of the X-ray observations of XMM J0038+40 used for our analysis. The flux limits quoted are the observed (i.e. absorbed) 0.2 – 10 keV 3σ limits in units of $\text{erg cm}^{-2} \text{s}^{-1}$, assuming the absorbed double black body model parameters given in Table 2. For the 2008 *XMM-Newton* observation in which XMM J0038+40 was detected, we give the absorbed flux in bold derived from the double blackbody model. For the two remaining *XMM-Newton* observations, the upper limit was only calculated for the pn image. The images for the *Swift* data taken in 2011 were summed together to increase signal-to-noise, so the upper limits are for the combined data. While the upper limits are quoted for each individual *ROSAT* observation, the limit from the summed observations is $3.9 \times 10^{-15} \text{ erg cm}^{-2} \text{ s}^{-1}$.

TABLE 4
LOG OF X-RAY OBSERVATIONS.

Telescope	ObsID	Date	Instrument	T_{exp}^a	Flux Upper Limit
<i>ROSAT</i>	600079N00	1991-07-14	PSPC	41.7	1.7×10^{-14}
<i>ROSAT</i>	600064N00	1991-07-15	PSPC	48.8	2.8×10^{-14}
<i>ROSAT</i>	141836N00	1992-01-12	PSPC	1.7	6.7×10^{-14}
<i>ROSAT</i>	141839N00	1992-01-13	PSPC	1.8	3.6×10^{-14}
<i>ROSAT</i>	141837N00	1992-01-13	PSPC	2.1	1.2×10^{-13}
<i>ROSAT</i>	600317N00	1992-07-20	PSPC	2.6	5.4×10^{-14}
<i>ROSAT</i>	600301N00	1992-07-22	PSPC	2.7	3.9×10^{-14}
<i>ROSAT</i>	600341N00	1992-07-23	PSPC	2.7	9.3×10^{-14}
<i>ROSAT</i>	600360N00	1992-07-23	PSPC	2.9	1.2×10^{-13}
<i>ROSAT</i>	600339N00	1992-07-25	PSPC	2.8	7.9×10^{-14}
<i>ROSAT</i>	600296N00	1992-07-25	PSPC	2.5	8.7×10^{-14}
<i>ROSAT</i>	600297N00	1992-07-25	PSPC	2.5	1.2×10^{-13}
<i>ROSAT</i>	600358N00	1992-07-26	PSPC	2.9	4.1×10^{-14}
<i>ROSAT</i>	600303N00	1992-07-27	PSPC	2.4	9.2×10^{-14}
<i>ROSAT</i>	600321N00	1992-07-29	PSPC	2.8	6.9×10^{-14}
<i>ROSAT</i>	600336N00	1992-07-29	PSPC	2.8	8.8×10^{-14}
<i>ROSAT</i>	600356N00	1992-08-03	PSPC	2.0	2.5×10^{-14}
<i>ROSAT</i>	600338N00	1992-08-03	PSPC	2.2	5.6×10^{-14}
<i>ROSAT</i>	600361N00	1992-08-05	PSPC	2.7	4.8×10^{-14}
<i>ROSAT</i>	600342N00	1992-08-05	PSPC	3.4	6.8×10^{-14}
<i>ROSAT</i>	600300N00	1992-08-05	PSPC	2.5	8.6×10^{-14}
<i>ROSAT</i>	600323N00	1992-08-05	PSPC	2.6	1.5×10^{-13}
<i>ROSAT</i>	600298N00	1992-08-05	PSPC	2.6	2.2×10^{-13}
<i>ROSAT</i>	600362N00	1992-08-06	PSPC	2.4	5.7×10^{-14}
<i>ROSAT</i>	600319N00	1992-08-06	PSPC	1.8	5.8×10^{-14}
<i>ROSAT</i>	600340N00	1992-08-06	PSPC	2.6	6.2×10^{-14}
<i>ROSAT</i>	600322N00	1992-08-06	PSPC	2.6	1.0×10^{-13}
<i>ROSAT</i>	600318N00	1992-08-06	PSPC	1.4	1.2×10^{-13}
<i>ROSAT</i>	600359N00	1992-08-06	PSPC	2.6	1.7×10^{-13}
<i>ROSAT</i>	600318a01	1992-12-21	PSPC	1.3	1.2×10^{-13}
<i>ROSAT</i>	600316N00	1992-12-21	PSPC	2.7	1.4×10^{-13}
<i>ROSAT</i>	600357N00	1992-12-30	PSPC	2.7	4.1×10^{-14}
<i>ROSAT</i>	600302N00	1992-12-30	PSPC	2.6	1.3×10^{-13}
<i>ROSAT</i>	600337N00	1992-12-30	PSPC	2.1	1.5×10^{-13}
<i>ROSAT</i>	600299a01	1993-01-01	PSPC	1.4	6.2×10^{-14}
<i>ROSAT</i>	600244N00	1993-01-02	PSPC	35.9	1.8×10^{-14}
<i>ROSAT</i>	600343N00	1993-01-04	PSPC	2.7	7.5×10^{-14}
<i>ROSAT</i>	600320a01	1993-07-01	PSPC	2.7	6.3×10^{-14}
<i>Chandra</i>	2046	2000-11-05	ACIS-S	14.8	1.6×10^{-14}
<i>Chandra</i>	2047	2001-03-06	ACIS-S	14.8	2.1×10^{-14}
<i>Chandra</i>	2048	2001-07-03	ACIS-S	14.0	1.4×10^{-14}

TABLE 4—*Continued*

Telescope	ObsID	Date	Instrument	T_{exp}^a	Flux Upper Limit
<i>XMM-Newton</i>	0402560101	2006-06-28	pn	44.1	4.2×10^{-15}
<i>Swift</i>	00035337001	2007-06-01	XRT	9.2	9.0×10^{-15}
<i>XMM-Newton</i>	0505760101	2007-07-24	pn	57.0	3.2×10^{-15}
<i>XMM-Newton</i>	0511380101	2008-01-02	pn	44.1	1.5×10^{-12}
<i>Swift</i>	00031919001	2011-02-04	XRT	2.9	3.3×10^{-14}
<i>Swift</i>	00031919002	2011-02-07	XRT	1.4	3.3×10^{-14}
<i>Swift</i>	00031919003	2011-02-11	XRT	0.9	3.3×10^{-14}
<i>Swift</i>	00031919004	2011-02-15	XRT	0.7	3.3×10^{-14}

^aExposure time in kiloseconds.